Precise measurement of the differential cross section from the16O(,)16O elastic reaction at 165° and 170° between 2.4 and 6.0 MeV

Demarche, Julien; Terwagne, Guy

Link to publication

Precise measurement of the differential cross section from the $^{16}O(\alpha,\alpha)^{16}O$ elastic reaction at 165° and 170° between 2.4 and 6.0 MeV

Julien Demarche[a)] and Guy Terwagne

Laboratoire d'Analyses par Réactions Nucléaires (LARN), University of Namur (FUNDP),
Rue de Bruxelles 61, B-5000 Namur, Belgium

Non-Rutherford cross section for elastic scattering of α particles from oxygen has been measured for energies between 2.4 and 6.0 MeV at commonly used backscattering angles of 165° and 170°. High precision in energy has been obtained with a 2 MV Tandetron accelerator, with precise and stable energy calibration. The choice of a thin $Ta_2O_5/Ta/C$ standard increased the sensitivity and reduced systematic errors due to the geometry. Precise data for energy, width, and ratio to Rutherford of the resonances have been extracted from nuclear shell models, and excitation levels of ^{20}Ne have been deduced. The well-known resonance $E_R = 3031.7 \pm 0.5$ keV and the narrow and intense resonance $E_R = 5375.5 \pm 0.5$ keV, not included in cross-section libraries, have been applied for surface oxygen analysis in thin $WCN/SiO_2/Si$ multilayer samples, with improved depth resolution by optimizing the measuring geometry. © *2006 American Institute of Physics.* [DOI: 10.1063/1.2402868]

I. INTRODUCTION

Rutherford backscattering spectroscopy (RBS) using 2 MeV α particles is a standard technique for the quantitative and nondestructive analysis of thin films. This technique is more sensitive to heavy elements as the cross section of elastic scattering is proportional to the square of the atomic number and usually used for depth profiling heavy elements in a matrix containing lighter elements. However, when high energy α particles are employed, the sensitivity for light elements can be substantially increased by the large enhancement of the elastic cross section resulting from nuclear reactions. When the incident beam energy is close to or higher than the Coulomb barrier of the target atoms, excitations in the nuclear levels can be induced and yield nuclear reactions or resonances. The resonant cross sections may exceed the Rutherford cross section by a factor of 10–100. As an example, the (α,α) cross section from ^{16}O for a backscattering angle of 170.5° at the resonance energy of 3.034 MeV has been reported to be 22.7 times the Rutherford cross section.[1]

The $^{16}O(\alpha,\alpha)^{16}O$ reaction has been widely investigated since the measurements made by Cameron in 1953.[2] The author reported five narrow resonances for energies between 2.4 and 3.9 MeV with an uncertainty on the energy of about 10 keV. For 50 years, many experimental and theoretical studies have been made for this specific reaction.[1–14] A major review covering the nuclear reactions used for oxygen analysis has also been published by Cohen and Rose.[15] The well-known resonance located at the energy of 3.034 MeV is suitable for depth profiling oxygen in materials. The energies and widths of the resonance are reported in Table I as well as the ratio to the Rutherford cross section. Disagreement amongst the results is observed especially in the position of the resonance energy, which has been reported between

3.030 MeV (Ref. 13) and 3.045 MeV.[2] Moreover, another very narrow resonance, which has been reported at $E_\alpha = 5.432$ MeV by McDermott *et al.*,[3] is not present in the cross-section library of the SIMNRA code.[16] Most of the accelerators used[1–14] are based on an electrostatic high voltage power supply, which means that the beam energy depends on the calibration of the magnets, which deviates the beam in the target chamber. The calibration depends strongly on the geometrical parameters of all elements included in the accelerator (source, low energy acceleration and/or high energy acceleration, magnet, and slits). In contrast, the uncertainty on the high voltage is only 100 V when set to 2 MV using a high voltage power supply based on the dynamitron process (Tandetron™) for which no slits are required. After a precise calibration of the high voltage, such accelerators show remarkable stability and reliability for up to a few years. In order to obtain optimal resolution with the $^{16}O(\alpha,\alpha)^{16}O$ resonance, we have measured the characteristics of that reaction with very high precision: the resonance energy E_R, the width Γ_{lab}, and the intensity relative to the Rutherford cross section σ/σ_R.

After the preparation of standards containing oxygen (Ta_2O_5) deposited on thin Ta substrates, we have measured the $^{16}O(\alpha,\alpha)^{16}O$ elastic reaction simultaneously at two backward angles (165° and 170°) for energies ranging from 2.4 to 6.0 MeV. Subsequently, the resolution of the resonance for a very thin oxide layer (~10 nm) was checked and the geometry optimized to increase the depth resolution.

II. STANDARD PREPARATION

Cross-section measurements require the use of standards containing a well known and large amount of oxygen. Tantalum oxide (Ta_2O_5) has all the qualities of a good standard: it is easily reproducible, it contains a large amount of oxygen (71 at. %), and it has a long-term stability under ion beam irradiation.[17] A thin tantalum oxide, formed by anodic oxida-

---

[a)]Electronic mail: julien.demarche@fundp.ac.be

100, 124909-1

TABLE I. Parameters of the $l=3$ resonance near 3.034 MeV for the $^{16}O(\alpha,\alpha)^{16}O$ cross-section.

θ_{lab}	E_R (keV)	Γ_{lab} (keV)	σ/σ_R	Accelerator type	Reference
164°	3045±10	10	29	VDG-electrostatic	2
154°	3036±2.3	10.12±0.37	6	VDG-electrostatic	5
164°	3042±3.0	10.2±0.4	15	VDG-electrostatic	6
165°	3042±3.0	10.26±0.49	15	VDG-electrostatic	8
170.5°	3034±4	10	22.5	VDG-electrostatic	9
165°	3037	21±1	14.4	Tandem-electrostatic	14
170°	3035±6	13	23.2	Tandem-electrostatic	10
150°	3030±5	12	8.5	Tandem-electrostatic	13

tion on a 600 nm Ta layer deposited on a glassy carbon substrate, was actually used for this study. The thickness of the Ta layer was chosen to ensure optimal sensitivity of the reaction. Figure 1 shows a spectrum recorded on the Ta_2O_5 standard at a backward angle of 170° for 3.045 MeV α particles, an energy region just above the well-known resonance located at $E_R=3.034$ MeV, but where the cross section of the $^{16}O(\alpha,\alpha)^{16}O$ is very low. It is clearly seen that the oxygen region is almost free of background contributions such that the sensitivity is increased. In Fig. 1, we have also plotted a simulation for a thick Ta substrate (solid gray line). The low-intensity oxygen peak would not be distinguished amongst experimental background.

A pure tantalum layer was first deposited by physical vapour deposition (PVD) on a polished glassy carbon disk (20 mm diameter). Carbon was chosen as the substrate in order to reduce the background under the oxygen peak to almost zero. This increases the sensitivity of the measurements especially for the energy regions where the cross section is very low.

Anodic oxidation of the tantalum coating was carried out as described by Amsel et al.[18] in an electrolyte solution consisting of triply distilled water with 5% ammonium citrate solution buffered to $pH=6$ with ammonia. However, in order to perform the anodic oxidation on the Ta thin coating deposited on glassy carbon, the oxidation cell described by Amsel et al. was slightly modified with a ring of copper
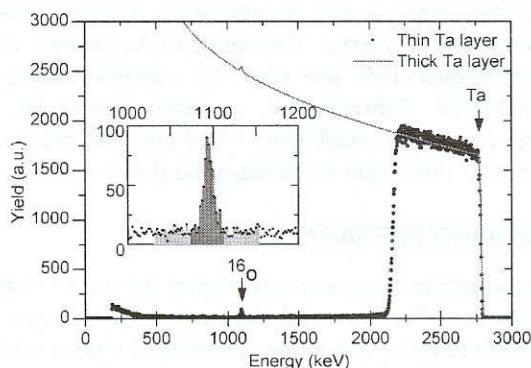
directly on the Ta/C anode (Fig. 2) in order to ensure good electrical contact.

We have prepared two Ta_2O_5 standards: a thin layer (~3 keV energy loss for $E_\alpha=3$ MeV) for probing resonance peaks and a thicker layer (~12 keV for $E_\alpha=3$ MeV) to scan regions where the cross section varies slowly. The thickness of both standards was measured with conventional RBS analysis at backward angles and 2 MeV α particles. The Ta_2O_5 stoichiometry was confirmed by x-ray photoelectron spectroscopy (XPS) measurements.

III. EXPERIMENTAL PROCEDURE

A. Accelerator energy calibration

The cross section of the $^{16}O(\alpha,\alpha)^{16}O$ reaction was measured between 2.4 and 6 MeV for two different angles with Accélérateur Linéaire Tandétron pour l'Analyse et l'Implantation des Solides (ALTAÏS), the 2 MV Tandetron™ accelerator installed at LARN (Namur, Belgium). In order to calibrate the voltage of the terminal, a large variety of (p,n) neutron threshold and nuclear resonant reactions induced by protons was used. These reactions, which cover the full range of accessible voltages of the tandem accelerator, are reported in Table II. The outgoing energy of the accelerated beam is given by the following formula:

$$E = (V_c + V_e + V_t)\frac{M}{M_{tot}} + qV_t, \qquad (1)$$

where V_c and V_e are, respectively, the cathode and the extraction voltages of the source of negative ions by cesium sputtering (SNICS), V_t is the theoretical terminal voltage, M and M_{tot} are, respectively, the masses of the outgoing cation and the incoming anion, and q the charge state of the outgo-

FIG. 1. Backscattering spectra for 3 MeV α particles on Ta_2O_5/Ta standards: experimental points on our thin Ta_2O_5/Ta (600 nm)/C standard (dots) and simulation for Ta_2O_5 on a thick Ta backing (solid gray line). In insert, the mean of the left and right backgrounds is subtracted from the oxygen peak to calculate the cross section.
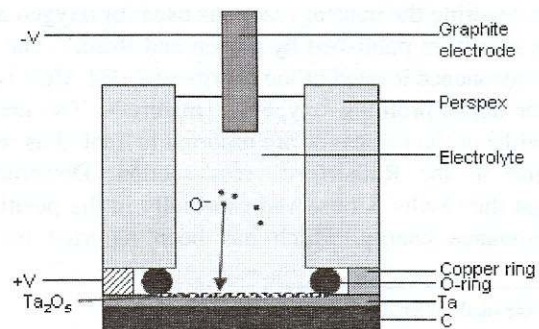

FIG. 2. Electrolytic cell for Ta/C anodic oxidation.

TABLE II. Nuclear reaction thresholds and resonances used for calibrating the terminal voltage of the Tandetron accelerator. V_t and V_{expt} are, respectively, the theoretical and the experimental voltages of the terminal.

Reaction	E_{th} or E_R (MeV)	V_t (kV)	V_{expt} (kV)	Reaction type
$^7Li(p,n)^7Be$	1.880 36	923.68	916.94	Threshold
$^9Be(p,n)^9B$	2.057 43	1012.215	1002.88	Threshold
$^{13}C(p,n)^{13}N$	3.235 57	1601.28	1587.96	Threshold
$^{19}F(p,\alpha\gamma)^{16}O$	0.340 46	153.73	152.42	Resonance
$^{19}F(p,\alpha\gamma)^{16}O$	0.872 11	419.555	416.58	Resonance
$^{15}N(p,\alpha\gamma)^{12}C$	0.429 00	198.00	197.00	Resonance

ing cation. Generally, the incoming anion and the outgoing cation have the same masses except for producing heavy ion beams with a very short lifetime, such as N⁻. In Table II, the theoretical terminal voltages V_t are compared to the terminal voltages actually applied, V_{expt} for ALTAÏS. A linear regression between V_t and V_{expt} gave a correlation coefficient of $R=1$ (Fig. 3). The relationship between theoretical and applied terminal voltages is given by

$$V_t = V_{expt} \times 1.0065(\pm 0.0003). \quad (2)$$

The excellent correlation means that the beam energy is not affected by the geometry of all elements included in the accelerator (source, low energy acceleration and/or high energy acceleration, magnet, and slits). Resonant reactions shown in Table II are regularly used for depth profiling elements in materials and good reproducibility is observed for the experimental voltage V_{expt}. The beam energy spread is given principally by the ripple of the high voltage terminal (~ 100 V), which means that the precision on the energy of the α beam is better than 0.4 keV.

B. Experimental details

We have measured the cross section of the $^{16}O(\alpha,\alpha)^{16}O$ reaction between 2.4 and 6.0 MeV simultaneously at two different angles $\theta = 165.0° \pm 0.5°$ and $\theta = 170.0° \pm 0.5°$. The α-particle beam, delimited by horizontal and vertical slits producing a square spot of 0.6×0.6 mm^2, impinged on the samples at normal incidence. When the cross section varied rapidly, an energy step of 1 keV was chosen and the measurements were realized with the thin Ta$_2$O$_5$ standard. On the contrary, the thicker Ta$_2$O$_5$ standard was used to explore the regions where the cross section varied slowly with energy steps of 20–100 keV. Backscattered α particles were detected in two passivated implanted planar silicon (PIPS) detectors with an active area of 25 mm^2 and a depleted zone of 700 μm. The energy resolution of the detectors subtending solid angles $\Omega = 4.0 \pm 0.1$ msr was typically 10 keV. Collimated cylinders were placed in front of each detector to reduce undesired background due to dual scattering in the target and the wall of the chamber.

Carbon contamination due to buildup is regularly observed when long irradiation times are necessary, especially when cross sections are measured over a large energy range. This phenomenon is especially due to the residual gas in the beam line, where the vacuum is typically 10^{-4} Pa. In order to
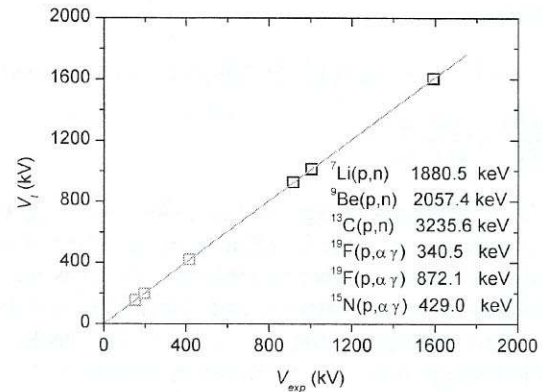

FIG. 3. (Color online) Theoretical voltage vs experimental voltage for the ALTAÏS Tandetron™ accelerator.

improve the statistics and obtain good precision, the integrated charge at each energy was typically limited to 20 μC where resonances are observed and 100 μC for the plateau where the cross section is low. We have taken into account the buildup of carbon by regularly measuring its content using the resonant reaction $^{12}C(\alpha,\alpha)^{12}C$ at $E_\alpha = 4.265$ MeV.[19] The evolution of carbon contamination versus integrated charge is presented in Fig. 4. The data represented by the same symbol correspond to the same beam spot on the target. A linear dependence is clearly observed such that the carbon concentration $N_C(10^{15}$ at. cm$^{-2})$ can be fitted by a straight line,

$$N_C = (0.150 \pm 0.006)Q, \quad (3)$$

where Q is the total integrated charge expressed in microcoulombs. The energy loss ΔE(eV) in the contamination layer is then calculated by

$$\Delta E = N_c \varepsilon, \quad (4)$$

where ε is the stopping cross section [eV/(10^{15} at./cm^2)]. Typical energy corrections were less than 1 keV. We have also regularly changed the position of the beam spot on the Ta$_2$O$_5$ standard to reduce the buildup of carbon contamination, especially where large variations in the cross section (resonances) were encountered.

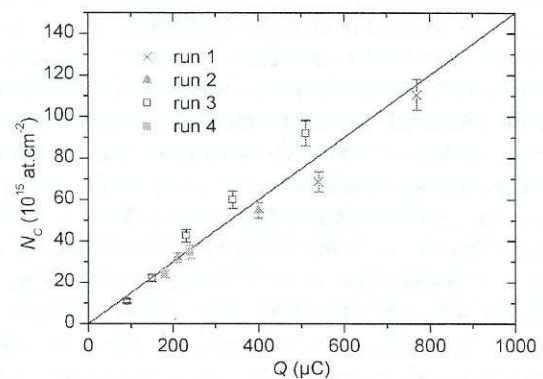FIG. 4. (Color online) Carbon buildup contamination (N_C) vs integrated charge (Q) during measurements. Each run refers to a different spot on the sample.

IV. RESULTS

The backscattering cross section was calculated using

$$\frac{d\sigma(E)}{d\Omega} = \frac{A_O \cos\theta_{in}}{\Omega N_i (Nt)_O}, \tag{5}$$

where E is the mean energy in the oxide layer, θ_{in} is the incident angle between the incident beam and the normal of the sample, N_i is the number of incident ions, Ω is the solid angle subtended by the detector, and $(Nt)_O$ is the number of oxygen atoms present in the Ta_2O_5 layer. The background under the oxygen peak was removed by selecting the mean background at the left and the right of the peak (Fig. 1), and the factor ΩN_i was calculated using the calculated Rutherford cross section on Ta,

$$\Omega N_i = \frac{A_{Ta} \cos\theta_{in}}{[d\sigma(\bar{E})/d\Omega]_{Ta}(Nt)_{Ta}}, \tag{6}$$

where A_{Ta} is the area under the Ta peak and $(Nt)_{Ta}$ is the number of tantalum atoms present in the oxidized layer. The scattering Rutherford cross section on Ta was calculated for the mean energy of α particles in the Ta coating. This approximation, which assumes that the particles have a mean energy in the entire Ta layer, leads to a negligible error, estimated at between 1% and 2%.

The backscattering cross section of α particles from ^{16}O is thus given by

$$\left[\frac{d\sigma(E)}{d\Omega}\right]_O = \frac{A_O}{A_{Ta}} \frac{(Nt)_{Ta}}{(Nt)_O} \left[\frac{d\sigma(\bar{E})}{d\Omega}\right]_{Ta}. \tag{7}$$

As we eliminate the main source of uncertainties (due to geometry), the precision on the cross section measured is enhanced. The statistical uncertainty on the oxygen peak is estimated to be in the range of 2%–5% and the error on the oxide layer thickness does not exceed 3%. So, the total imprecision on the cross section is typically 4%–8%. The precision of the energy provided by the Tandetron accelerator ALTAÏS and the correction made on the energy loss in the carbon contamination layer allow us to reduce the uncertainty associated with the energy to below 0.4 keV.

The measured differential cross section for backscattering angles of 165° and 170° are presented in Figs. 5(a) and 5(b), respectively. For energies below 4.0 MeV, five narrow resonances are located at energies of 2475.0, 3031.7, 3073.0, 3363.3, and 3870.8 keV. It is clearly observed that the resonance at $E_R = 3031.7$ keV is more intense at 170°. This angle should be preferred for depth profiling oxygen with high sensitivity. Below 4 MeV, the heights of the plateaus observed between the resonances are close to the Rutherford cross section [dashed lines in Figs. 5(a) and 5(b)]. For energies higher than 4 MeV, the intensity of the differential cross sections is increased due to very broad resonances at energies around 4.6 and 5.15 MeV, respectively. Narrow resonances are also observed for energies between 4.9 and 5.5 MeV, located, respectively, at energies of 4958.0, 5139.0, 5375.5, and 5470.0 keV. The resonance observed at 5375.5 keV is very narrow (2.5 keV) and could be used to detect the presence of oxygen at an interface with very high
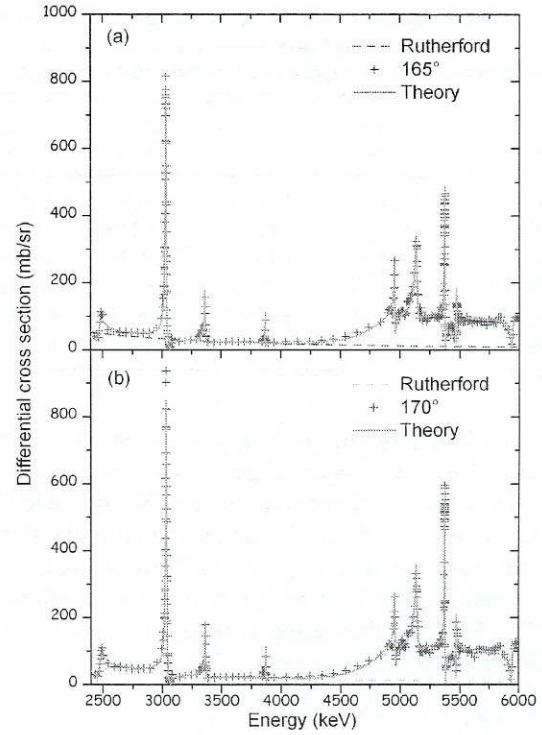

FIG. 5. (Color online) Experimental and theoretical differential cross sections of the $^{16}O(\alpha, \alpha)^{16}O$ reaction at laboratory angles of (a) 165° and (b) 170° for α-particle energies varying from 2.4 to 6.0 MeV.

resolution. Plateaus are also observed between the resonances but the height of the cross section in the flat regions is ten times the differential Rutherford cross section.

V. DISCUSSION

Figures 6 and 7 show details of the differential cross section divided by the Rutherford cross section commonly referred to as the *ratio to Rutherford cross section*, for energies around the 3.0317 MeV resonance, which is the new adopted energy value, and energies between 4.9 and 5.5 MeV. The results compared to the data obtained, respectively, by Feng et al.[14] and Cameron[2] in Fig. 6(a) show disagreement in the position as well as in amplitude. The ratio to Rutherford cross section measured at 170° [Fig. 6(b)] is compared to the data obtained at 170° and 170.5° by Leavitt et al.[1] and Cheng et al.[10] respectively. In this case, a small disagreement (~2 keV) in the resonance energy is observed while the amplitudes are almost identical. For the resonances located between 4.9 and 5.5 MeV, a large disagreement in energy (~50 keV) is observed in Fig. 7(a) between our data and the measurements reported by McDermott et al. at $\theta_{cm} = 168.9°$,[3] which corresponds to $\theta_{lab} = 165.2°$. The resonances observed by Feng et al. are located between our data and the measurements of McDermott et al. Again large discrepancies in amplitude are observed for the measurements done by Feng et al. At 170°, the comparison of our data and the measurements of Cheng et al. is very good with respect to the position of the resonances and for the amplitude except for the narrow resonance located at 5.3755 MeV, which is completely absent from the measurements of Cheng et al. This resonance has only been observed by McDermott et al.[3]
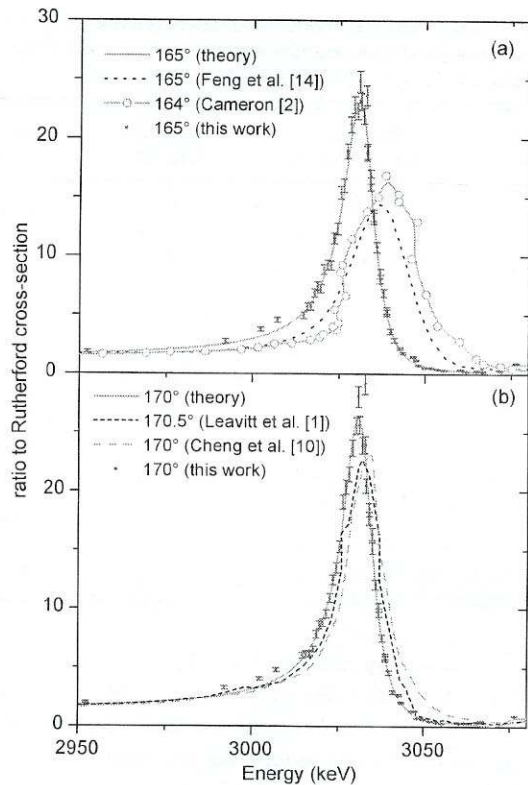
FIG. 6. (Color online) Experimental and theoretical ratio to Rutherford cross section around the $E_R = 3031.7$ keV resonance compared to results reported by other authors at laboratory angles of (a) 165° and (b) 170°.

at 165° but the position in energy was completely wrong.

The quality of our measurements allows us to calculate the energy levels of ^{20}Ne with very high precision (<0.5 keV). We have used the RES5 code, which is a program included in the RUMP package[20] to calculate the resonant scattering cross section based on nuclear shell models (solid line in Figs. 5–7). The results are presented in Table III. The values of the excited state of ^{20}Ne are calculated relatively to the ground state, evaluated from the masses given by Audi et al.[21] The energies of the levels are in very

TABLE III. Resonances observed for the ^{16}O$(\alpha, \alpha)^{16}$O reaction between 2.4 and 6.0 MeV.

| E_α^a (keV)	Γ_{lab}^a (keV)	Γ_{cm}^a (keV)	E_x^a (keV)	E_x^b (keV)	Γ_x^b (keV)	ΔE (keV)	J^π
2475.0±0.5	60	48	6709.4	6725	19.0	15.6	0+
3031.7±0.4	13	10.4	7154.7	7156.3	8.2	1.6	3−
3073.0±0.5	7.0	5.6	7187.7	7191	3.4	3.3	0+
3363.3±0.4	10	8.0	7419.9	7421.9	15.1	2.0	2+
3870.8±0.5	1.0	0.8	7825.8	7829.0	2	3.2	2+
~4900±50	~3000	~2400	8649	~8700	>800	51	0+
4958.0±0.5	8.0	6.4	8695.4	8708	2.1	12.6	1−
5058.0±0.5	0.11	0.09	8775.4	8777.6	0.1	2.2	6+
~5100±10	~1400	~1120	8809	~8800	>800	9	2+
5139.0±0.5	20	16	8840.2	8854	19	13.8	1−
5375.5±0.5	2.5	2.0	9029.4	9031	3.0	1.6	4+
5470.0±0.5	3.5	2.8	9105.0	9116	3.2	11	3−
5940.0±0.5	25	20	9480.9	9487	29	6.1	2+

[a]This work.
[b]Reference 22.
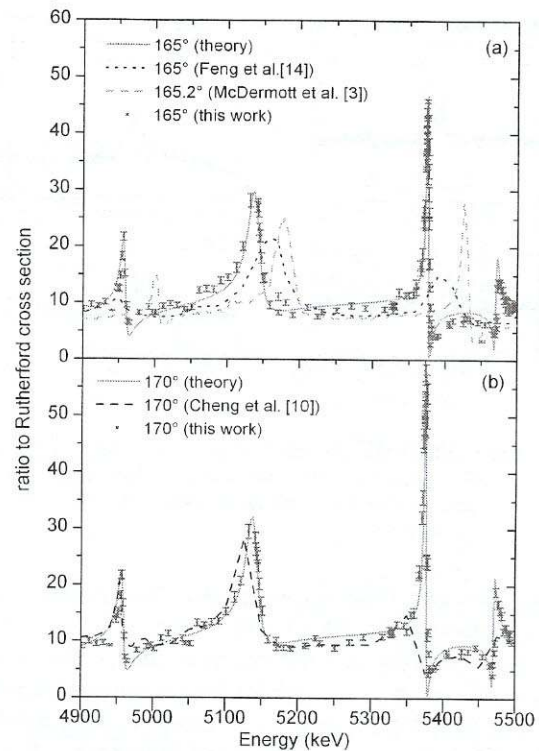
FIG. 7. (Color online) Experimental and theoretical ratios to Rutherford cross section between 4.9 and 5.5 MeV compared to results reported by other authors at laboratory angles of (a) 165° and (b) 170°.

good agreement with the compiled results given by the *Table of Isotopes*,[22] taking into account the new values of the resonance energies and the refining of the ^{20}Ne ground state energy with recent mass values.

VI. EXAMPLES OF APPLICATION

The ^{16}O$(\alpha, \alpha)^{16}$O resonances are of considerable interest for depth profiling oxygen in matrices containing heavy elements. The resonances located at $E_R = 3031.7$ and 5375.5 keV are so narrow that it is possible to depth profile oxygen at an interface of a multilayer sample.

We have checked the limits of the performance of the ^{16}O$(\alpha, \alpha)^{16}$O reaction by making backscattering analysis on a sample of WCN/SiO$_2$/Si (100), with layer thicknesseses of 40 and 10 nm for WCN and SiO$_2$, respectively. We wished to investigate the oxygen contamination at the surface of the WCN layer.

The energy loss for 3 MeV α particles is about 9.5 keV in the WCN layer and 2.8 keV in SiO$_2$, i.e., smaller than the width of the $E_R = 3031.7$ keV resonance. At this energy, surface and depth contributions from the SiO$_2$ layer would not be resolved. We have nevertheless increased the depth resolution by optimizing the detection geometry.

Two PIPS detectors, collimated as described in Sec. III B, were placed symmetrically in the chamber, for backscattering angles $\theta = 170°$. The target was tilted at an angle $\alpha = 60°$ from the incident beam. The experimental spectra recorded by the two detectors for a beam energy $E_R = 3031.7$ keV could then be compared in Fig. 8. By tilting the target at 60°, the number of atoms encountered by α particles is doubled, and the depth resolution is improved. In
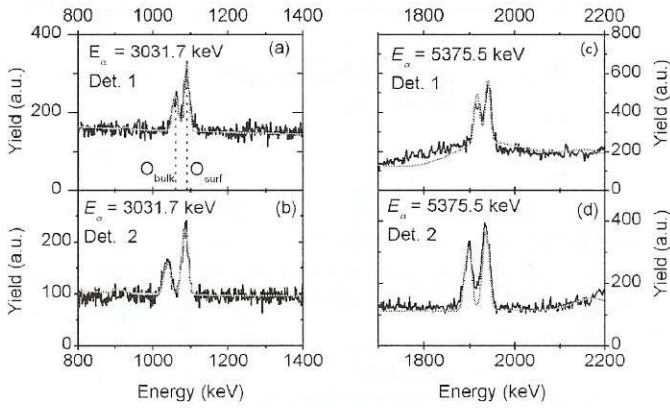
FIG. 8. (Color online) Oxygen peaks in the experimental backscattering spectra of WCN (40 nm)/SiO$_2$ (10 nm)/Si at an energy of 3031.7 keV for (a) detector 1 and (b) detector 2 and at an energy of 5375.5 keV for (c) detector 1 and (d) detector 2.

TABLE IV. Composition and thicknesses of layers determined by the use of the tilted target method with detection opposite to the tilt and $^{16}O(\alpha, \alpha)^{16}O$ resonances at $E_R = 3031.7$ keV and $E_R = 5375.5$ keV.

Layer	Thickness (10^{15} at. cm^{-2})	Element	Concentration (at. %)
1	48.91	C	100.0
2	84.08	W	17.0
		C	26.6
		N	11.9
		O	44.54
3	130.47	W	38.2
		C	25.2
		N	36.6
4	90.58	Si	25.38
		O	74.62
5	Substrate	Si	100

Fig. 8(a), we can observe two peaks corresponding to the surface contamination (O$_{surf}$) and to the SiO$_2$ layer (O$_{bulk}$). The depth resolution can also be enhanced by the detection geometry. The path of α particles backscattered towards detector 2 is 38% higher than for detector 1. As a result, the 29 keV shift between the surface and bulk peaks of oxygen in detector 1 is increased to 47 keV on the experimental spectrum from detector 2 [Fig. 8(b)]. As the two peaks are clearly distinguished, with no oxygen signal in between, they can unambiguously be attributed to the SiO$_2$ layer and to a thin surface contamination layer of oxygen. The tilted target method coupled with a two detector setup thus showed clear advantages to improve the depth resolution in the case of thin multilayer samples.

At $E_R = 5375.5$ keV, stopping powers of α particles are lower. Particles lose 7.0 keV in the WCN layer and 1.9 keV in SiO$_2$. With a width $\Gamma = 2.5$ keV, the intense resonance permits easily discrimination of oxygen from the surface and the bulk [Fig. 8(c)]. The $\alpha = 60°$ tilt coupled with detection in the opposite direction was nevertheless chosen to enhance the depth resolution [Fig. 8(d)]. Although accuracy was limited by the strongly non-Rutherford Si background, good agreement between experimental and fitted spectra could be obtained.

The enhancement factor of the resonant cross section thus allows easy quantification of oxygen, notwithstanding the superposition of the peak with the Si substrate background. By increasing the energy, a depth profile is obtained. The increased sensitivity of backscattering spectroscopy added to the improved depth resolution of the tilted target method thus allowed the determination of the thickness and composition of layers, using the SIMNRA 6.0 code (Table IV).

VII. CONCLUSIONS

The measurement of the differential cross section from the $^{16}O(\alpha, \alpha)^{16}O$ elastic reaction, at energies of 2.4–6.0 MeV and at backscattering angles of 165° and 170°, is of a fundamental and applied interest. Due to the high precision calibration of the energy given by ALTAÏS, the energies of the resonances have been accurately determined with a precision of one order of magnitude below the mea-

surements realized by other authors. The ratio to the Rutherford cross section has been moreover precisely measured, by using a thin Ta$_2$O$_5$/Ta/C standard, which allowed us to increase the sensitivity and reduce the systematic errors due to the geometry.

We have given new resonance parameters E_R and Γ obtained by fitting experimental data with a theoretical curve from nuclear shell models. The energies and the widths of the resonances have been precisely measured, especially for the very thin resonances located, respectively, at 3031.7 and 5375.5 keV. The measured parameters are in very good agreement with the adopted values.[22] Excitation levels of ^{20}Ne have been then refined from these data.

The use of the thin resonances has been applied in backscattering analysis. The precise knowledge of the resonance parameters allows precise depth profiling of oxygen at interfaces from matrix of heavy elements. This has been demonstrated in the frame of surface oxygen analysis of thin WCN/SiO$_2$/Si samples. Tilting the target and detecting in the opposite direction increase depth resolution with the well-known $E_R = 3031.7$ keV resonance. The narrow and intense resonance at $E_R = 5375.5$ keV, which was not referenced in previous papers, has also been investigated as an oxygen probe. The results in extreme conditions show great prospects for BS analysis of oxygen.

[1]J. A. Leavitt, L. C. McIntyre, M. D. Ashbaugh, J. G. Oder, Z. Lin, and B. Dezfouly-Arjomandy, Nucl. Instrum. Methods Phys. Res. B **44**, 260 (1990).
[2]J. R. Cameron, Phys. Rev. **90**, 839 (1953).
[3]L. C. McDermott, K. W. Jones, H. Smotrich, and R. E. Benenson, Phys. Rev. **118**, 175 (1960).
[4]J. John, J. P. Aldrige, and R. H. Davies, Phys. Rev. **181**, 1455 (1969).
[5]J. D. MacArthur, H. C. Evans, J. R. Leslie, and H. B. Mak, Phys. Rev. C **22**, 356 (1980).
[6]Z. L. Wang, J. F. M. Westendorp, and F. W. Saris, Nucl. Instrum. Methods Phys. Res. **211**, 193 (1983).

[7] F. Michel, J. Albinski, P. Belery, Th. Delbar, Gh. Grégoire, B. Tasiaux, and G. Reidemeister, Phys. Rev. C **28**, 1904 (1983).

[8] R. A. Jajris, Nucl. Instrum. Methods Phys. Res. B **12**, 331 (1985).

[9] J. A. Leavitt, P. Stoss, D. B. Cooper, J. L. Seerveld, L. C. McIntyre, R. E. Davies, S. Gutierrez, and T. M. Reith, Nucl. Instrum. Methods Phys. Res. B **15**, 296 (1986).

[10] H. Cheng, H. Shen, J. Tang, and F. Yang, Nucl. Instrum. Methods Phys. Res. **83**, 449 (1983).

[11] F. Michel, G. Reidemeister, and Y. Kondo, Phys. Rev. C **51**, 3290 (1995).

[12] Z. S. Zheng, J. R. Liu, X. T. Cui, and W. K. Chu, Nucl. Instrum. Methods Phys. Res. B **118**, 449 (1996).

[13] W. Jiang, V. Shutthanandan, S. Thevuthasan, D. E. McReady, and W. J. Weber, Nucl. Instrum. Methods Phys. Res. B **207**, 453 (2003).

[14] Y. Feng, Z. Y. Zhou, Y. Y. Zhou, and G. Q. Zhao (unpublished).

[15] D. D. Cohen and E. K. Rose, Nucl. Instrum. Methods Phys. Res. B **66**, 158 (1992).

[16] M. Mayer, AIP Conf. Proc. **475**, 541 (1999).

[17] M. P. Seah *et al.*, Nucl. Instrum. Methods Phys. Res. B **30**, 140 (1988).

[18] G. Amsel, J. P. Nadai, C. Ortega, S. Rigo, and J. Siejka, Nucl. Instrum. Methods **149**, 705 (1978).

[19] J. A. Leavitt, L. C. McIntyre, P. Stoss, J. G. Oder, M. D. Ashbaugh, B. Dezfouly-Arjomandy, Z. M. Yang, and Z. Lin, Nucl. Instrum. Methods Phys. Res. B **40–41**, 776 (1989).

[20] L. R. Doolittle, Nucl. Instrum. Methods Phys. Res. B **9**, 344 (1985).

[21] G. Audi, A. H. Wapstra, and C. Thibault, Nucl. Phys. A **728**, 337 (2003).

[22] R. B. Firestone, V. S. Shirley, C. M. Baglin, J. Zipkin, and S. Y. F. Chu, *Table of Isotopes*, 8th ed. (Wiley-Interscience, Berkeley, 1996), p. 415.